Trade-off between the control bandwidth and the measurement accuracy in Atomic Force Microscopy

Stefan Kuiper, Paul Van den Hof
Delft Center for Systems and Control
Delft University of Technology
Mekelweg 2, 2628 CD,Delft, The Netherlands.
Email: stefan.kuiper@tudelft.nl, p.m.j.vandenhof@tudelft.nl

Georg Schitter
Automation and Control Institute
Vienna University of Technology
Gusshausstrasse 27-29, A-1040, Vienna, Austria.
Email: schitter@acin.tuwien.ac.at
(corresponding author)

***Abstract*—In Atomic Force Microscopy the force between the tip and the sample is controlled in a feedback loop in order to prevent damage to the tip and the sample during scanning, and also to convert the force measurement into an estimate of the sample topography. In this paper it is experimentally shown that within the design of the control system a direct trade-off has to be made between the bandwidth of the feedback loop and the accuracy of the topography estimation due to the dynamical uncertainty of the systems. Several method are suggested to reduce the dynamical uncertainty of the imaging system to allow both faster and more accurate AFM imaging. Moreover, a method is discussed and experimentally validated to compensate for the loss in imaging accuracy due to the hysteresis within the piezoelectric actuators.**

I. Introduction

In Atomic Force Microscopy (AFM) [1], the sample topography is measured by probing the sample with a very sharp tip, while scanning the sample or tip in a raster scan-pattern. The measurement tip is mounted on the free end of a micro-cantilever which allows to measure the interaction force between the tip and the sample during imaging. The nonlinear tip sample interaction force is controlled in a feedback loop for two reasons: (i) to prevent damage of the tip and the sample during imaging, and (ii) to provide an estimate of the sample topography. In order to provide the scanning motion and to allow the control of the tip sample force, a positioning stage is used which can position the tip relative to the sample in all three spatial directions.

A major challenge in AFM development is to improve its relatively low-imaging speed, taking in the order of several minutes per frame for most commercially available systems nowadays [2]. This has motivated a vast amount of research on improving both the achievable scanning speed, as well as improving the bandwidth of the feedback loop that controls the tip sample interaction force [3], [4], [5], [6]. Meanwhile, the consequences of the increased control bandwidth on the accuracy of the instruments has not been investigated in much detail. Improved topography estimation has been investigated by taking into account a model of the dynamical behavior of the system [7], [8], [9]. However, the dynamical behavior of the system may show some variations when changing the tip, sample or imaging conditions, which poses strong limitations on the achievable control bandwidth and the accuracy of the topography estimation. Recently, a new method has been proposed for integrated design of the feedback controller and topography estimator, while taking into account the dynamical uncertainties of the system [10]. In this contribution, the application of the integrated design method of [10] is demonstrated on a commercially available AFM system, and the influence of the dynamical uncertainty of the system on the topography estimation accuracy is validated experimentally.

Section II discusses the topography estimation problem and how the accuracy of the topography estimation depends on the design of the feedback controller. This is discussed and analyzed for a commercially available AFM in Section III, and experimental validation is shown in Section IV. In Section V several steps are suggested to reduce the dynamical uncertainty of the system, and a method to compensate for the hysteresis in the piezoelectric actuator is demonstrated. Conclusions are drawn in Section VI.

II. Topography Estimation in AFM

Figure 1 shows a block diagram of the feedback loop in AFM, with G the actuator dynamics, P the sensor dynamics, and K the feedback controller. While scanning, the sample topography enters the feedback loop as an unknown disturbance signal denoted $h(t)$ in Figure 1. The feedback controller is tracking this topography variation via the actuator. In Laplace domain this is given as:

$$X(s) = -\frac{L(s)}{1+L(s)} \cdot H(s) = E(s) - H(s); \qquad (1)$$

with $L(s) = P(s) \cdot K(s) \cdot G(s)$ the loop gain of the control loop. $H(s)$, $X(s)$ and $E(s)$ are the Laplace transforms of the topography signal $h(t)$, the actuator displacement $x(t)$, and the control error $e(t)$ respectively.

In most commercially available AFM-systems a calibrated scaling of the control signal $u(t)$ is taken as a measure of the sample topography. However, for higher bandwidth and more accurate sample topography estimation the cantilever deflection signal $d(t)$, and the system dynamics should be taken into account [7], [8], [9]:

$$\hat{H}(s) = \underbrace{\hat{P}^{-1}(s) \cdot D(s)}_{\hat{E}(s)} - \underbrace{\hat{G} \cdot U(s)}_{\hat{X}(s)}, \qquad (2)$$

978-1-4577-1772-7/12/$26.00 ©2012 IEEE

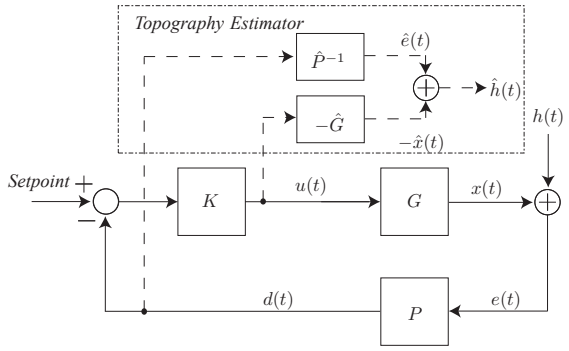

Figure 1. Block diagram of the vertical feedback loop in AFM, with actuator dynamics G, sensor dynamics P, and feedback controller K. The topography estimator provides an estimate of the topography signal $h(t)$ based on sensor signal $d(t)$ and control signal $u(t)$.

with $\hat{P}(s)$ a model of the sensor dynamics $P(s)$, and $\hat{G}(s)$ a model of the actuator dynamics $G(s)$. Combining (1) and (2), the topography estimation error can be calculated as:

$$\begin{aligned}\varepsilon(s) &= \hat{H}(s) - H(s) = \Big[\hat{E}(s) - E(s)\Big] - \Big[\hat{X}(s) - X(s)\Big] \\ &= \Big[\hat{P}(s)^{-1} \cdot D(s) - E(s)\Big] - \Big[\hat{G}(s) \cdot U(s) - X(s)\Big] \qquad (3) \\ &= \frac{\Big[P(s)\hat{P}^{-1}(s) - 1\Big] - P(s)K(s)\Big[\hat{G}(s) - G(s)\Big]}{1 + L(s)} \cdot H(s),\end{aligned}$$

This transfer function reveals that the topography estimation error is partly stemming from the modeling error of the sensor dynamics $[P(s) \cdot \hat{P}^{-1}(s) - 1]$, and partly stemming from the modeling error of the actuator dynamics $[\hat{G}(s) - G(s)]$. Important is also to note the influence of the feedback controller $K(s)$ in Equation (3), determining the propagation of the modeling errors towards the topography estimation error.

A difficulty in the modeling of the system dynamics is that some dynamic variations may occur when changing the sample, measurement tip, or the imaging conditions. As a consequence, the system contains some dynamical uncertainty which limits the achievable accuracy of the topography estimate. Recently, an integrated design methodology is proposed to design the feedback controller $K(s)$ and topography estimator model $\hat{G}(s)$, explicitly taking into account the influence of the dynamical uncertainty of the system [10]. In the following this integrated design strategy is applied on a commercially available AFM system, and experimentally validated via two design cases with different control bandwidths.

III. Design example and analysis

The experimental setup used in this research is based on a commercially available AFM-system (Multimode V, Bruker Nano Inc., Santa Barbara, USA), which utilizes a piezoelectric tube scanner ('J-scanner') to position the sample in all three spatial directions. In order to identify the dynamical behavior of the system and its variations, the system is prepared several times using different sample discs with masses ranging from 0.5 to 1 gram, and by varying the alignment of the sample disc on the actuator. The actuator responses are measured by using a network analyzer (4395A, Agilent, Santa Clara, USA). By only using cantilevers with high free resonance frequencies ($\geq$ 300 kHz) in contact mode, the sensor dynamics can be considered static below 100 kHz, which is the frequency range of interest. Therefore, the sensor dynamics P are neglected in the following analysis, and for convenience and easier comparison the gain from actuator input $u(t)$ to cantilever deflection signal $d(t)$ is normalized. The results of two different frequency response measurements are shown in Figure 2a (solid red and dashed blue lines), clearly showing the first longitudinal resonance of the piezoelectric tube scanner at 8 kHz. The various measurements clearly reveal the variations in the dynamical behavior associated with the different load conditions [11].

For the model-based controller design a 7th order dynamical model $G_n(s)$ is fitted based on the data of 12 different frequency response measurements, to capture the nominal dynamical behavior of the system, as is shown by the dashed-dotted lines of Figure 2. Based on this nominal model the maximum multiplicative modeling error can determined at each frequency point

$$\Psi(\omega_f) = \max_{j=1\ldots k} \left| \frac{\Phi_j(\omega_f) - G_n(\omega_f)}{G_n(\omega_f)} \right|, \qquad (4)$$

with $\Phi_j(\omega_f)$ the j^{th} measured frequency response of the actuator dynamics, and with $j = 1 \ldots k$ the number of recorded frequency response measurements. The maximum multiplicative modeling error is shown by the solid line of Figure 2b and shows that the dynamical uncertainty tents to become larger at higher frequency. In order to capture the dynamical uncertainty into the model set, a 5th order overbounding filter $Q(s) \geq \Psi(\omega_f)$ is fitted as shown by the dashed line of Figure 2b. As discussed in [10] the accuracy of the topography estimate can be explicitly addressed in the design of the feedback controller, by penalizing the excitation of the dynamical uncertainties of the system, governed the by weighting filter Q(s). In the sequel of the paper two design cases are compared, both designed according to the design procedure proposed in [10]: one design case denoted '*LB*' in which higher emphasis is put on the accuracy of the topography estimate, and one design case denoted '*HB*' in which a high control bandwidth is considered more important. Figures 3a shows the Bode magnitude plots of the nominal sensitivity function for both design cases, with a disturbance rejection bandwidth of about 400 Hz for design case *LB* (solid, black), and 1 kHz for design case *HB* (dashed, red). Meanwhile, Figure 3b shows the worst-case magnitude of the transfer function towards the topography estimation error $\frac{\epsilon(\omega_f)}{H(\omega_f)}$ analyzed at each frequency point for both design cases. These graphs are obtained by substituting the designed feedback controller K, the model of the nominal actuator dynamics $\hat{G}$, and the set of all frequency response measurements $\Phi_n(\omega_f)$ into Equation 3, and assuming the sensor dynamics to be static and normalized, i.e. $\hat{P} = P = 1$:

$$\max \left| \frac{\epsilon(\omega_f)}{H(\omega_f)} \right| = \max_{j \in [1\ldots k]} \left| \frac{K(\omega_f)[\Phi_j(\omega_f) - \hat{G}(\omega_f)]}{1 + K(\omega_f)\Phi_j(\omega_f)} \right|.$$

Figures 3 shows that for design case *LB* the accuracy of the topography estimate is better as compared to design case *HB*, particulary at higher frequencies. This is explained by the fact that with the lower control bandwidth in design case *LB* also the excitation of the uncertain dynamics is lower, which improves the accuracy of the topography estimation. Hence, Figures 3 clearly reveals the design trade-off between the control bandwidth of the system, and the accuracy of the topography estimate.

IV. Experimental results

In order to demonstrate the trade-off between the bandwidth and the accuracy of the system experimentally, the feedback controllers are implemented on the AFM system by means of a *Field-Programmable-Gate-Array* (FPGA, Virtex-II Pro XtremeDSP Development Kit, Nallatech, Camarillo CA, USA). In order to facilitate the implementation, the 15th order controllers obtained from the controller synthesis are reduced via balanced truncation to 10th and 8th order for the lower and higher bandwidth designs respectively. The controllers are discretized to a sampling rate of 260 kHz, and implemented on the *FPGA* in a biquad structure. The implementation of the (model-based) topography estimator is done offline, by recording the signals via the data channels of the AFM controller, and filtering the data with the designed estimator model in `matlab Simulink`.

In order to isolate the topography estimation errors stemming from the dynamical uncertainty of the system from other error sources such as scanner drift in the lateral plane, an arbitrary topography signal is added to the cantilever deflection signal using an analog summing amplifier, while the scanning motion of the system is disabled. As this arbitrary topography signal is fully known, this allows to accurately judge the topography estimation errors stemming from the dynamical uncertainty of the system, as obtained with the different feedback controllers and topography estimators.

Figure 4 shows the measured results when applying a 200 Hz block wave signal with an amplitude of 250 nm as a topography signal to the system, controlled with either the low bandwidth or the high bandwidth feedback controller. Figure 4 shows the output of the feedback controller $u(t)$ (Fig. 4a), the measured tracking error signal from the photodiode $d(t)$ (Fig. 4c), the estimated sample topography $\hat{h}(t)$ (Fig. 4b), and the topography estimation error $\epsilon(t) = \hat{h}(t) - h(t)$ (Fig. 4d), for the systems corresponding to both design cases. The graphs of Figure 4a and 4c clearly reveal that the system controlled by the high bandwidth controller (design case *HB*) provides a better tracking of the topography signal. These experiments are repeated several times (data not shown), while varying the load conditions on the scanner showing similar for all cases. For this particular topography signal the RMS value of the tracking error is calculated to be about 30% lower with design case *HB* as compared to the design case *LB*. In contrast, Figure 4d reveals that with design case *LB* the topography estimation errors are significantly smaller (40% RMS) as compared to design case *HB*. Hence, the results of Figure 4 clearly confirm the trade-off between the tracking bandwidth, and the accuracy of the topography estimate. Analyzing the periodicity of the topography estimation error reveals that a significant fraction of the topography estimation error is stemming from the dynamical uncertainty around the lateral resonance at 1 kHz, which confirms the frequency domain analysis of the dynamic uncertainty shown in Figure 3b.

V. Reducing the dynamical uncertainty

The results discussed in the previous section clearly show that the dynamical uncertainty of the imaging system limits both the achievable control bandwidth of the tip-sample interaction force, as well as the accuracy of the topography estimation. Therefore, in order to allow both faster and more accurate AFM imaging, in future designs the dynamical uncertainty of the system should be reduced. In order to reduce the dynamical uncertainty of the system the following design improvements are proposed:

Reducing load variations

The identification results of Figure 2 clearly shows that a significant amount of dynamical uncertainty is stemming from the varying weight and alignment of the sample discs on the scanner. Especially the varying alignment has a large influences as it strongly determines the coupling of the lateral resonance mode toward the displacement in z. Therefore, the dynamical consistency may be improved by introducing an indexing system that fixes the alignment of the sample discs on the scanner. Moreover, standardizing the weight of the sample discs would also reduce the dynamical uncertainty.

Damping the lateral resonance modes

The results of Figure 4 clearly reveal that a large fraction of the topography estimation error is stemming from the dynamical uncertainty associated with the coupling of the the first lateral resonance mode at 1 kHz towards the displacement in z direction. This dynamical uncertainty may be significantly reduced by damping these lateral resonance modes, for instance via active feedback control [12], [13], which is even possible without dedicated position sensors as discussed in [14].

Compensating for hysteresis

Although not explicitly addressed in the design of the linear control system discussed in the previous section, the piezoelectric actuators used in AFM typically suffer from hysteresis which may cause a certain amount of dynamical uncertainty if not accounted for. Depending on the quality of the piezo material this hysteresis may result in gain variations of about 1%, as in the case shown in Figure 7, up about 15%. An approach to this problem is to invert the non-linear hysteretic behavior via a Preisach hysteresis model [15]. However, in order to guarantee the accuracy of such a hysteresis model the full actuation history should be known, and the model may require frequent calibration. The hysteresis may also be compensated for by utilizing a charge controlled

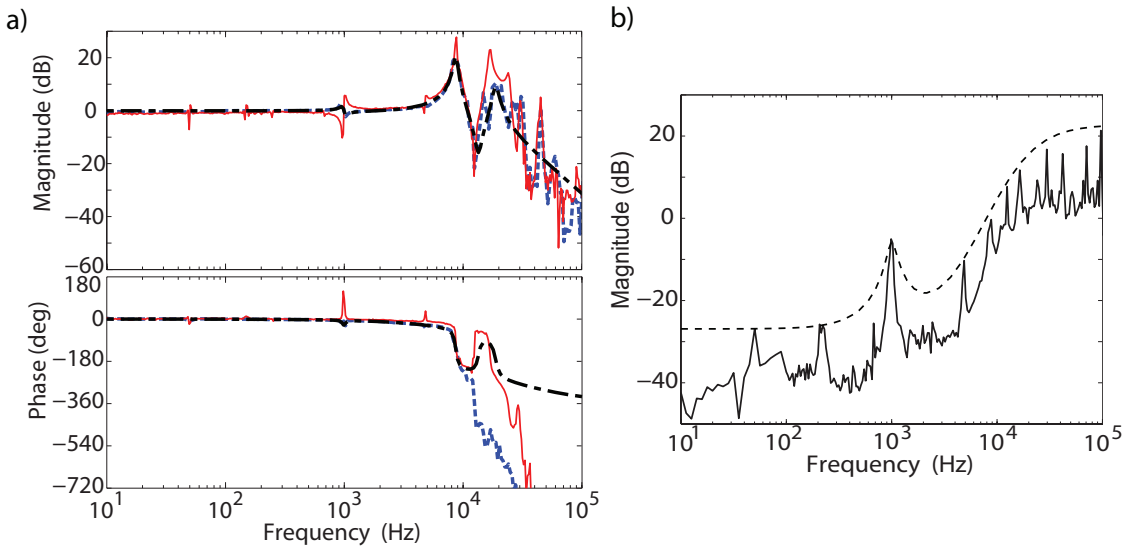

Figure 2. (a) Frequency response of the tube scanner measured in two different identification experiments (solid, red), and (dashed blue), and the frequency response of the fitted 7th order model (dashed-dotted, black) (b) the maximum multiplicative modeling error (solid, black) as a function of frequency, and the error over-bounding filter $Q(s)$ (dashed, black).

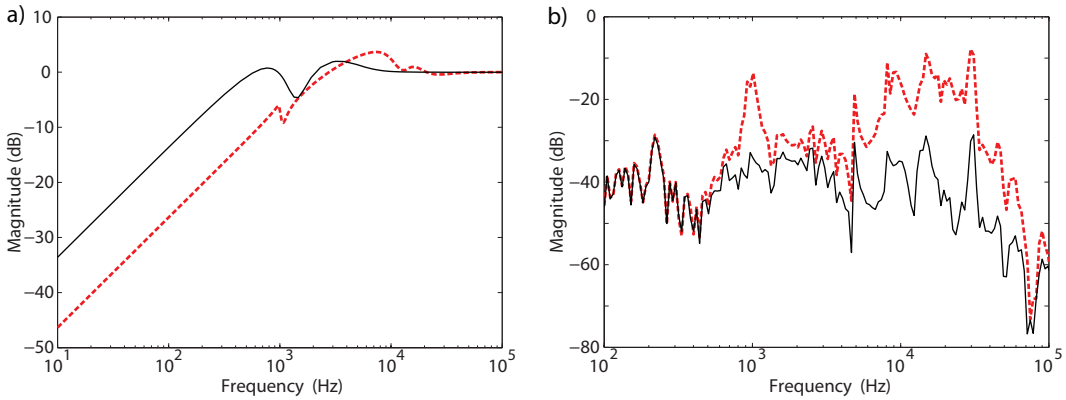

Figure 3. Frequency response plot of the nominal sensitivity function (a), and the worst-case topography estimation error determined at each frequency point for the closed-system (b), for design case *LB* (solid, black) and for design case *HB* (dashed, red).

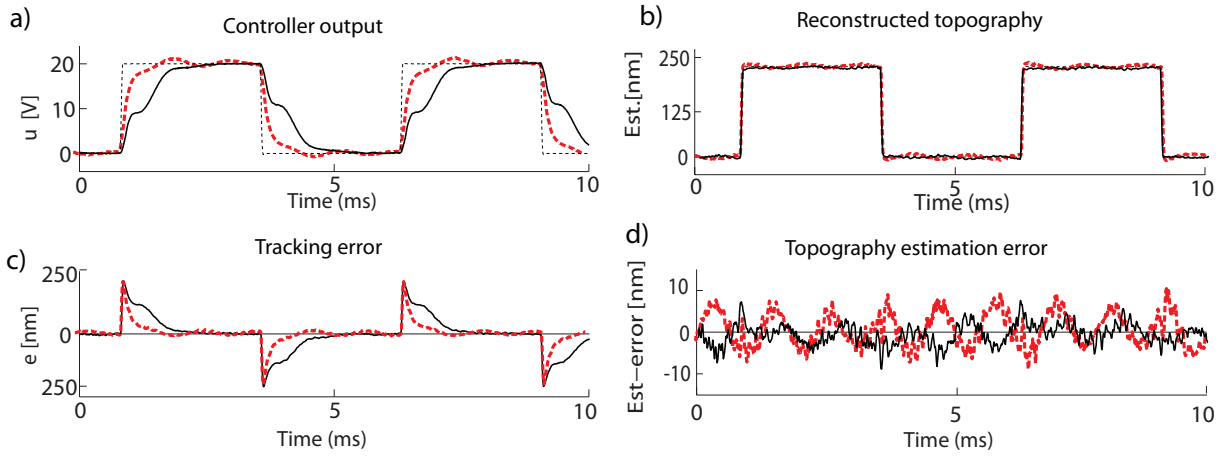

Figure 4. System outputs when applying a 200 Hz, 250 nm block wave signal as an artificial topography signal, for the system with a low-bandwidth controller (design case *LB*, (solid, black lines)), and for system with a high bandwidth controller (design case *HB*, (dashed, red lines)). Figure (a) shows the applied artificial reference signal $h(t)$ (dashed, black) together with the output of the feedback controller $u(t)$, while figure (c) shows the measured control error $d(t)$. Figure (b) shows the outputs of the topography estimator $\hat{h}$, and Figure (d) show the topography estimation error $\epsilon(t) = \hat{h}(t) - h(t)$.

amplifier [16], [17], making use of the fact that the hysteresis is not present in the relation between the charge and the displacement of the piezoelectric actuator [18]. However, applying charge control requires thorough redesign of the driving amplifier, and may suffer from larger noise and possible stability issues particulary at low frequencies.

Instead of linearizing the piezo actuators, the degrading effects of hysteresis on the accuracy of the topography estimate may also be compensated for by observing the hysteresis via a charge measurement, and taking this measurement into account in the topography estimator, as shown in Figure 5. The charge flowing through the piezoelectric actuator may be measured via the circuit as shown in Figure 6, measuring the voltage over a relatively large capacitor which is connected in series with the piezo element.

In order to validate the compensation of the hysteresis via a charge meaurement, the circuit of Figure 6 is implemented on the piezoelectric tube scanner used in the previous experiments. The displacement of the piezoelectric tube scanner in z direction is measured via a capacitive position sensor (6810 gaging module with a 6504-01 probe, ADE Technologies, Westwood, USA). Figure 7 shows the results when driving the system with a sinusoidal input signal of 50 Hz with an amplitude of ± 180 V, resulting in a total displacement of the piezoelectric actuator of about 4.5 μm. Figure 7a depicts the input voltage versus the actuator displacement, showing that the forward motion does not exactly overlap the backward motion due to the hysteresis. The maximum width and height of the hysteresis curve is about 0.05 μm at about 5 V, and thuss the gain variations due to the hysteresis are less than 1.5% at full displacement range. Figure 7b depicts the measured charge versus the actuator displacement, revealing no hysteresis in the relation between the measured charge and the actuator displacement. Hence, these results indicate that although the hysteresis of the piezoelectric actuator used in this system is relatively low, using the charge measurement as an input to the topography estimator instead of the input voltage compensates for the hysteresis and thus results in a better accuracy of the topography estimation. Especially AFM system utilizing piezoelectric stack actuators [4] typically suffer from a relatively high amount of hysteresis of up to about 15%, and therefore the dynamical uncertainty may be considerably reduced and the topography estimation accuracy of such systems may be significantly improved via the a charge measurement.

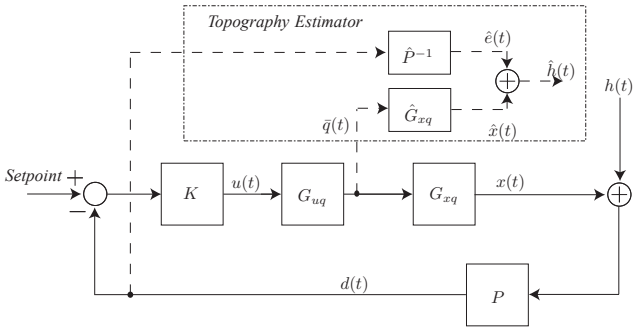

Figure 5. Block diagram of the feedback loop controlling the tip sample force in AFM with an additional charge measurement as input for the topography estimator. The actuator dynamics from input $u(t)$ towards the charge $q(t)$ are given by G_{uq}, and the actuator dynamics from charge $q(t)$ towards the actuator displacement $x(t)$ are given by G_{qx}. The topography estimator estimates the sample topography based on the cantilever deflection signal $d(t)$ and the measured charge $\bar{q}(t)$.

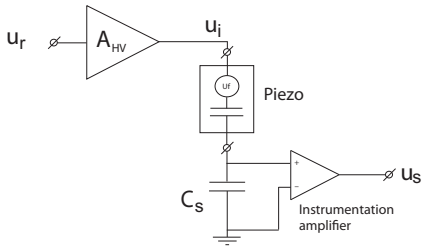

Figure 6. Circuit to measure the charge within the piezoelectric element for the compensation of hysteresis in the topography estimate. The charge within the piezo element is directly proportional to the voltage measured over the reference capacitor: $q(t) = C_s \cdot u_s(t)$.

VI. Conclusions

In this contribution it is experimentally demonstrated that the uncertain dynamics in AFM require a design trade-off between the bandwidth of the instrument to follow the sample topography, and the guaranteed bounds on the topography estimation error (i.e. the accuracy of the instrument). Several methods are suggested to reduce the dynamical uncertainty of the system to allow both faster and more accurate AFM imaging. Also a method is discussed to compensate for the loss in imaging accuracy due to the hysteresis within piezoelectric actuator by monitoring the charge instead of the voltage applied to the actuator.

These results suggest that when designing the feedback controller in AFM the intended imaging applications of the instrument have to be considered. When imaging for instance fragile biological samples, minimizing the force variations between the tip and the sample may be more important in order not to damage the sample, aiming for an as high as possible control bandwidth and therefore the requirements on the accuracy of the topography estimation may be somewhat relaxed. However, in other application such as quality assurance in the semiconductor industry, higher emphasis might be given on the quality of the topography estimation. Samples from material science or potentially semiconductors are not as fragile as biological systems, and higher importance may be given to the metrological aspects of the instrument. The integrated design method demonstrated in this contribution can be used to handle this design trade-off and optimize the feedback controller and topography estimator of the system to the particular imaging application.

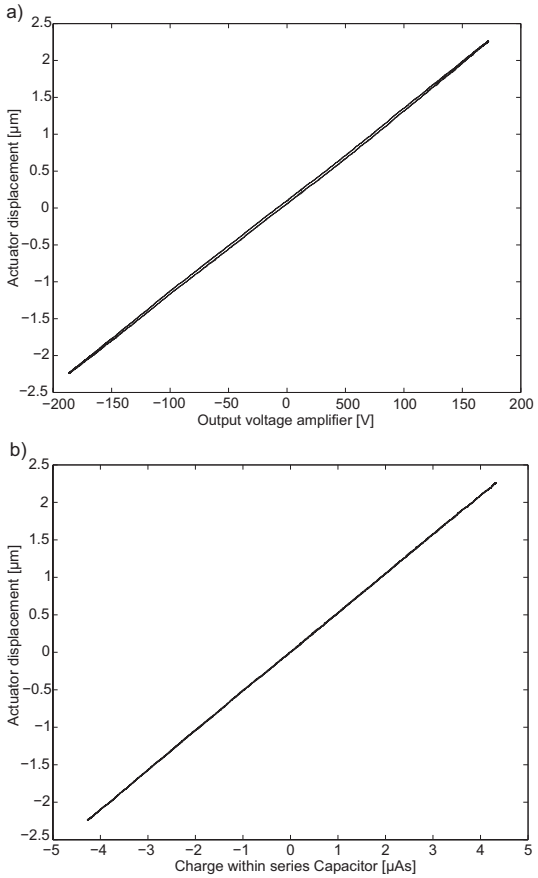

Figure 7. Identification of the hysteresis within the z-axis of the piezoelectric tube scanner ('J-scanner', Bruker Nano Inc., Santa Barbara, USA), showing the input voltage versus actuator displacement (a), and charge versus actuator displacement (b), in response to a 50 Hz 360 V_{pp} sinusoidal input signal.

VII. Acknowledgements

The authors would like to thank Dominik Kohl of the Vienna University of Technology for his help with the charge measurement experiments.

References

[1] G. Binnig, C. Quate, and C. Gerber, "Atomic force microscope," *Physical Review Letters*, vol. 56, no. 9, pp. 930–933, 1986.

[2] P. Hansma, G. Schitter, G. Fantner, and C. Prater, "High speed atomic force microscopy," *Science*, vol. 314, pp. 601–602, 2006.

[3] T. Ando, N. Kodera, E. Takai, D. Maruyama, K. Saito, and A. Toda, "A high-speed atomic force microscope for studying biological macromolecules," *Proceedings of the National Academy of Sciences*, vol. 98, no. 22, pp. 12 468–12 472, 2001.

[4] G. Schitter, K. Aström, B. DeMartini, P. Thurner, K. Turner, and P. Hansma, "Design and modeling of a high-speed afm-scanner," *IEEE Transactions on Control Systems Technology*, vol. 15, pp. 906–915, 2007.

[5] S. Devasia, E. Eleftheriou, and S. Moheimani, "A survey of control issues in nanopositioning," *IEEE Transactions on Control Systems Technology*, vol. 15, pp. 802–823, 2007.

[6] J. Butterworth, L. Pao, and D. Abramovitch, "A comparison of control architectures for atomic force microscopes," *Asian Journal of Control*, vol. 11, no. 2, pp. 175–181, 2009.

[7] G. Schitter, P. Menold, H. Knapp, F. Allgöwer, and A. Stemmer, "High performance feedback for fast scanning atomic force microscopes," *Review of Scientific Instruments*, vol. 72, p. 3320, 2001.

[8] S. Salapaka, T. De, and A. Sebastian, "A robust control based solution to the sample-profile estimation problem in fast atomic force microscopy," *International Journal of Robust and Nonlinear Control*, vol. 15, no. 16, pp. 821–838, 2005.

[9] C. Lee and S. Salapaka, "Fast imaging with alternative signal for dynamic atomic force microscopy," *Applied Physics Letters*, vol. 97, p. 133101, 2010.

[10] S. Kuiper, P. Van den Hof, and G. Schitter, "Towards integrated design of a robust feedback controller and topography estimator for atomic force microscopy," in *Proceedings of the 18th IFAC World Congress, Milan, Italy*, 2011, pp. 12 709–12 714.

[11] J. van Hulzen, G. Schitter, P. Van den Hof, and J. van Eijk, "Dynamics, load balancing, and modal control of piezoelectric tube actuators," *Mechatronics (in press)*, 2011.

[12] S. Salapaka, A. Sebastian, J. Cleveland, and M. Salapaka, "High bandwidth nano-positioner: A robust control approach," *Review of Scientific Instruments*, vol. 73, pp. 3232–3241, 2002.

[13] B. Bhikkaji, M. Ratnam, A. Fleming, and S. Moheimani, "High performance control of piezoelectric tube scanners," *IEEE Transactions of Control Systems Technology*, vol. 15, pp. 853–866, 2007.

[14] S. Kuiper and G. Schitter, "Active damping of a piezoelectric tube scanner using self-sensing piezo actuation," *Mechatronics*, vol. 20, pp. 656–665, 2010.

[15] D. Croft, G. Shed, and S. Devasia, "Creep, hysteresis, and vibration compensation for piezoactuators: Atomic force microscopy applications," *AMSE Journal of Dynamic Systems, Measurement, and Control*, vol. 123, pp. 35–43, 2001.

[16] H. Adriaens, W. De Koning, and R. Banning, "Modeling piezoelectric actuators," *IEEE/ASME Transactions on Mechatronics*, vol. 5, no. 4, pp. 331–341, 2000.

[17] A. Fleming, "Quantitative SPM topographies by charge linearization of the vertical actuator," *Review of Scientific Instruments*, vol. 81, no. 10, pp. 103 701(1–5), October 2010.

[18] M. Goldfarb and N. Celanovic, "Modeling piezoelectric stack actuators for control of micromanipulation," *IEEE Control Systems Magazine*, vol. 17, no. 3, pp. 69–79, 1997.